

STATISTICS OF X-RAY FLARES OF SAGITTARIUS A*: EVIDENCE FOR SOLAR-LIKE SELF-ORGANIZED CRITICALITY PHENOMENA

YA-PING LI¹, FENG YUAN^{1,2}, QIANG YUAN³, Q. DANIEL WANG³, P. F. CHEN⁴,
JOSEPH NEILSEN^{5,6}, TAOTAO FANG¹, SHUO ZHANG⁷, AND JASON DEXTER⁸¹ Department of Astronomy and Institute of Theoretical Physics and Astrophysics, Xiamen University, Xiamen, Fujian 361005, China; leeyp2009@gmail.com² Shanghai Astronomical Observatory, Chinese Academy of Sciences, 80 Nandan Road, Shanghai 200030, China; fyuan@shao.ac.cn³ Department of Astronomy, University of Massachusetts, Amherst, MA 01003, USA; yuanq@umass.edu, wqd@astro.umass.edu⁴ School of Astronomy and Space Science, Nanjing University, Nanjing 210023, China⁵ Boston University Department of Astronomy, Boston, MA 02215, USA⁶ MIT Kavli Institute for Astrophysics and Space Research, Cambridge, MA 02139, USA⁷ Columbia Astrophysics Laboratory, Columbia University, New York, NY 10027, USA⁸ Max Planck Institute for Extraterrestrial Physics, P.O. Box 1312, Giessenbachstr., D-85741 Garching, Germany

Received 2015 June 9; accepted 2015 July 21; published 2015 August 25

ABSTRACT

X-ray flares have routinely been observed from the supermassive black hole at our Galactic center, Sagittarius A* (Sgr A*). The nature of these flares remains largely unclear, despite many theoretical models. In this paper, we study the statistical properties of the Sgr A* X-ray flares by fitting the count rate (CR) distribution and the structure function of the light curve with a Markov Chain Monte Carlo method. With the 3-million-second *Chandra* observations accumulated in the Sgr A* X-ray Visionary Project, we construct the theoretical light curves through Monte Carlo simulations. We find that the 2–8 keV X-ray light curve can be decomposed into a quiescent component with a constant CR of 6×10^{-3} count s⁻¹ and a flare component with a power-law fluence distribution $dN/dE \propto E^{-\alpha_E}$ with $\alpha_E = 1.65 \pm 0.17$. The duration–fluence correlation can also be modeled as a power law $T \propto E^{\alpha_{ET}}$ with $\alpha_{ET} < 0.55$ (95% confidence). These statistical properties are consistent with the theoretical prediction of the self-organized criticality system with the spatial dimension $S = 3$. We suggest that the X-ray flares represent plasmoid ejections driven by magnetic reconnection (similar to solar flares) in the accretion flow onto the black hole.

Key words: accretion, accretion disks – black hole physics – Galaxy: center – methods: statistical

1. INTRODUCTION

Sagittarius A* (Sgr A*) at the center of the Milky Way is an excellent laboratory for studying the accretion and ejection of matter by supermassive black holes (SMBHs). There have been quite a number of observational and theoretical studies of Sgr A* (see reviews by Genzel et al. 2010 and Yuan & Narayan 2014). The bolometric luminosity of Sgr A* is $L_{\text{bol}} \sim 10^{-9} L_{\text{Edd}}$ (where L_{Edd} is the Eddington luminosity), which is five orders of magnitude lower than that predicted by a standard thin disk accretion at the Bondi accretion rate (Baganoff et al. 2003). We now understand that an advection-dominated accretion flow scenario works for Sgr A*, and that the low luminosity is due to the combination of the low radiative efficiency and the mass loss via outflow (Yuan et al. 2003, 2012; Narayan et al. 2012; Li et al. 2013; Wang et al. 2013; Yuan & Narayan 2014). Sgr A* is usually in a quiescent state, and occasionally shows rapid flares (on timescales ~ 1 hr), most significantly in X-ray (Baganoff et al. 2001) and near-infrared (NIR; Genzel et al. 2003; Ghez et al. 2004). The flare rate is roughly once per day in X-ray and more frequently in NIR.

Theoretical interpretations of the flares include the electron acceleration by, e.g., shocks, magnetic reconnection, or turbulence, produced in either an accretion flow (e.g., Yuan et al. 2004; Eckart et al. 2006; Dodds-Eden et al. 2009, 2010; Yusef-Zadeh et al. 2009; Chan et al. 2015) or in an assumed jet (e.g., Markoff et al. 2001). The other scenarios in terms of the flaring cause are transient features in the accretion flow, such as accretion instability (Tagger & Melia 2006), orbiting hot spot (Broderick & Loeb 2005), expanding plasma blob (Eckart et al.

2006; Yusef-Zadeh et al. 2006, 2009; Trap et al. 2011), and tidal disruption of asteroids (Zubovas et al. 2012). However, the nature of the flares is still under debate.

Before 2012, only about a dozen X-ray flares were detected (e.g., Baganoff et al. 2001; Porquet et al. 2003; Bélanger et al. 2005; Eckart et al. 2006; Aharonian et al. 2008; Marrone et al. 2008; Porquet et al. 2008; Yusef-Zadeh et al. 2008; Degenaar et al. 2013). Thanks to the *Chandra* X-ray Visionary Project on Sgr A* (hereafter XVP⁹) in 2012, a total of 39 flares have been added (Nielsen et al. 2013). This substantially increased sample size of flares has enabled the statistical study of the properties. Nielsen et al. (2013) first analyzed the distributions of the fluences, durations, peak count rates (CRs), and luminosities of the XVP detected flares. Nielsen et al. (2015) further investigated the flux distribution of the XVP X-ray light curves taking into account the Poisson fluctuations of the quiescent emission and the flare flux statistics.

In this work we advance the statistical analysis of the XVP light curve by simultaneously using its flux distribution and structure function (SF). We generate X-ray light curves through Monte Carlo realizations of both the quiescent and flare contributions. The realization of flares assumes power-law models for their fluence function and width-fluence dependence. The parameters of these power laws are in turn constrained by comparing the simulated data with the observed one, using the Markov Chain Monte Carlo (MCMC) approach.

The major motivation of the statistical analysis is to determine whether the self-organized criticality (SOC) model

⁹ <http://www.sgra-star.com/>

can explain Sgr A* X-ray flares, and if so to probe the dimensionality of the process leading to the flares. We compare our constrained power-law indexes (i.e., the power-law indexes for the fluence distribution and the duration-fluence correlation) with the expectation of the SOC theory, which describes a class of dynamical systems with nonlinear energy dissipation that is slowly and continuously driven toward a critical value of an instability threshold (Katz 1986; Bak et al. 1987; Aschwanden 2011; see the Appendix for a brief introduction to SOC and the relevant statistical method to be used in the present work). The energy dissipation driven by magnetic reconnection is believed to be in an SOC system, such as solar flares (Lu & Hamilton 1991), possibly the X-ray flares of γ -ray bursts (GRBs) and black holes of various scales (Wang & Dai 2013; Wang et al. 2015). An SOC system experiences scale-free power-law distributions of various event parameters, such as the total energy (or equivalently the fluence), the peak energy dissipation rate, the time duration, and the flux (or equivalently the CR) of events. These statistical properties are related to the geometric dimension of the system that drives the events, and can thus be used to diagnose their physical nature (Aschwanden 2012, 2014). While the statistical analysis of solar flares suggests a spatial dimension $S = 3$, consistent with the complex magnetic structure observed in active regions on the Sun (e.g., Priest & Forbes 2000), the X-ray flares of GRBs favor $S = 1$ (Wang & Dai 2013). Thus, it is argued that the X-ray flares occur in the jets of GRBs where the magnetic field configuration tends to be poloidal and thus one-dimensional (Wang & Dai 2013). Wang et al. (2015) further claim $S = 3$ from an analysis of the X-ray flares of Sgr A*, Swift J1644+57, and M87. However, this analysis is very crude in the sense that the correlation among different bins of the cumulative distribution are not properly addressed, that artificial cuts of the fitting range of the data are adopted, and that the used flare sample is strongly biased and incomplete at the detection limit (Wang 2004). All these issues are handled in the present work.

The rest of this paper is organized as follows. The observational data and the statistical method adopted are described in Section 2. We present the fitting results in Section 3, and discuss the physical implication of the results in Section 4. Finally we conclude this work in Section 5.

2. DATA AND METHODOLOGY

2.1. Observations

We use the data of the 2012 *Chandra* XVP campaign, which consists of 38 *Chandra* ACIS-S/HETGS observations of Sgr A* with a total exposure time of 3 million seconds (Ms) between 2012 February 6 and October 29. The 2–8 keV light curve is extracted in 300 s bins including both photons of the 0th order and the ± 1 st diffraction orders. The 0th order events are extracted from a circle region with a radius of $1''.25$, while the ± 1 st order events are extracted from a $2''.5$ rectangular region (Nielsen et al. 2013). For more details of the XVP campaign and data reduction, we refer the readers to Nielsen et al. (2013).

¹⁰ This modeling is used as the 1st-order approximation to account for the correlation among photons from individual flares, although some bright ones do show significant asymmetric shapes (Baganoff et al. 2001; Nowak et al. 2012), and/or substructures (Barrière et al. 2014).

2.2. Synthetic Light Curve

The X-ray light curve can be decomposed into the quiescent and flare components. The quiescent emission is assumed to be steady with a CR r . We model the flare component as a sum of Gaussian functions.¹⁰ Then the model light curve is

$$R(t) = \sum_{i=1}^{[\kappa]} \frac{E_i}{\sqrt{2\pi}\sigma_i} \exp\left[-\frac{1}{2}\left(\frac{t - \mu_i}{\sigma_i}\right)^2\right] + r, \quad (1)$$

where E_i , σ_i , and μ_i are the fluence, width, and peak location of the i th flare, $[\kappa]$ is the integer part of κ and it presents the total number of flares. We use a Monte Carlo method to generate the model light curve, which accounts for the Poisson fluctuations of photon counting. The differential flare fluence function is assumed to be a power-law form,

$$dN/dE \propto \begin{cases} E^{-\alpha_E}, & E_{\min} \leq E \leq E_{\max} \\ 0, & \text{otherwise} \end{cases}, \quad (2)$$

where the lower limit of the fluence $E_{\min} = 1$ cts is well below the detectable flare fluence in Nielsen et al. (2013), and the upper limit $E_{\max} = 1000$ cts is slightly larger than that of the brightest flare (Nowak et al. 2012). Given α_E and κ , the fluences of the model flares can be easily sampled.

As shown in Nielsen et al. (2013), there is a clear correlation between the flare fluence E and duration T (defined as four times the Gaussian width σ). We characterize this correlation with a log-normal distribution $N(\log \sigma_i, \sigma_{ET})$, where σ_{ET} is the Gaussian dispersion and a power-law relation between σ_i and E_i as

$$\sigma_i = A \left(\frac{E_i}{100}\right)^{\alpha_{ET}} \quad (3)$$

where A is the normalization constant and α_{ET} is the power-law index.¹¹ The intrinsic scattering of the flare widths around the power-law relation is estimated to be $\sigma_{ET} = 0.25$ for the detected sample (Q. Yuan et al. 2015, in preparation). The peak time μ_i of each flare is generated randomly in the observational periods. The discrete light curve is then generated in 300 s bins, resulting in $M = 9964$ bins for the total exposure of the data. The average CRs are calculated in each bin of the simulated light curve. In total we will have five parameters to describe the synthetic light curve, namely the Poisson background r , the power-law index of the fluence distribution α_E , the total flare number κ , the duration normalization A , and the fluence-duration correlation slope α_{ET} .

Finally we correct the pileup effect of the simulated light curve by assuming the 1st-order CRs a constant fraction, 52%, of the incident rate (Nowak et al. 2012, see also Nielsen et al. 2013, 2015). For all the simulated CRs, the pileup correction is less than 20%.

Figure 1 shows a representative simulated light curve (blue), compared with the observational one (red) with the observing gaps removed.

¹¹ In this work we use α_X to represent the power-law index of the distribution of variable X (specifically $dN/dX \propto X^{-\alpha_X}$), and α_{XY} to represent the correlation power-law index between X and Y (specifically $Y \propto X^{\alpha_{XY}}$).

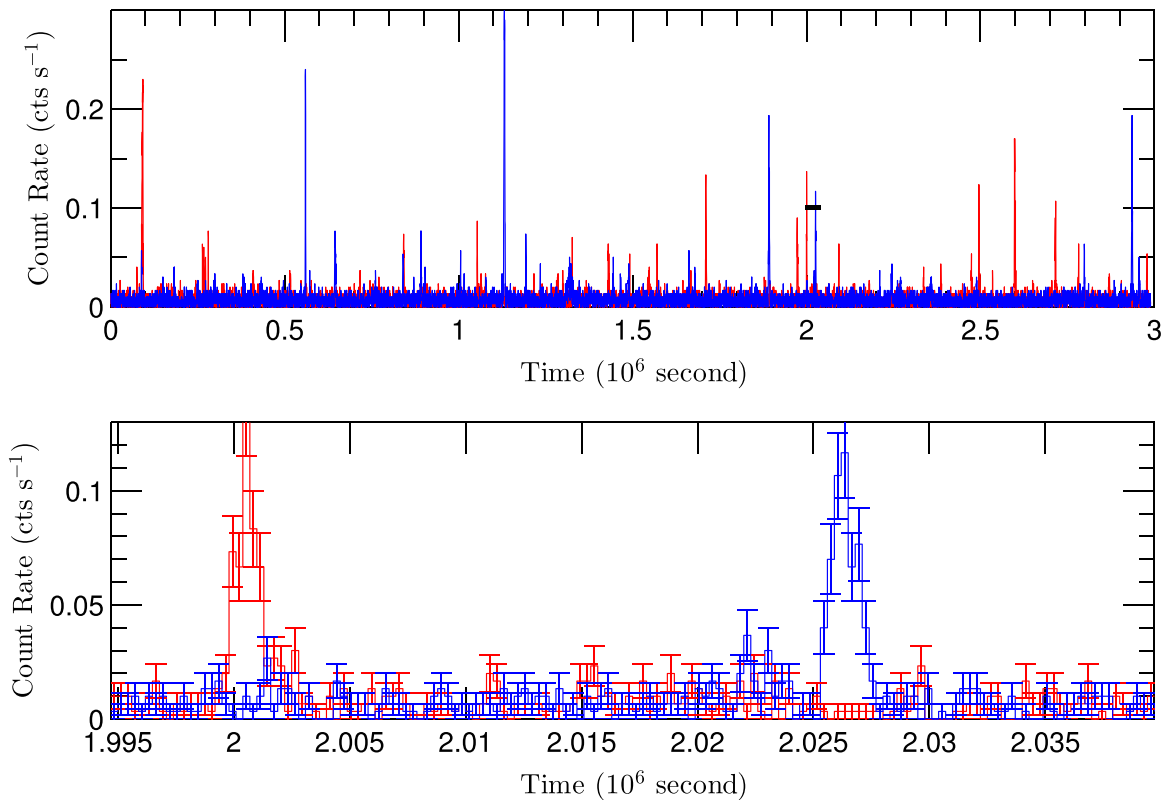


Figure 1. Upper panel: the light curve (with the observing gaps removed) from the XVP observations (red), compared with a representative one from the simulations (blue) using the best-fit parameters of model I shown in Table 1 (see below). Lower panel: zoomed-in light curve of a time window indicated by the short horizontal bar in the upper panel.

2.3. Statistical Comparison

The synthetic light curve cannot be directly compared to the observational one due to the lack of bin-to-bin correspondence between the two. We need a statistical way to make the comparison. A “first” order statistic is the CR distribution, which reveals the overall magnitude of the variabilities. However, as mentioned above (also noted in Neilsen et al. 2015), the CR distribution contains no information about the flare flux correlation among adjacent bins. This correlation can be independently accounted for by the use of the auto-correlation function, or equivalently the SF for a stationary process (Simonetti et al. 1985; Emmanoulopoulos et al. 2010). We jointly fit the CR distribution and the SF to determine the model parameters.

2.3.1. CR Distribution

With the 300 s bins both for the simulated and observed data, the binning results in $M = 9964$ data points for the total exposure window. We construct the CR distribution of the data logarithmically and follow Knuth (2006; see also Witzel et al. 2012) to determine the optimal bin number of the histogram. Considering the histogram as a piecewise-constant model, the relative logarithmic posterior probability (RLPP) for the bin number m , given M data points, is

$$\text{RLPP}(m) = M \log m + \log \Gamma\left(\frac{m}{2}\right) - m \log \Gamma\left(\frac{1}{2}\right) - \log \Gamma\left(M + \frac{m}{2}\right) + \sum_{l=1}^m \log \Gamma\left(n_l + \frac{1}{2}\right), \quad (4)$$

where n_l is the histogram value of the l th bin, and $\Gamma(x)$ is the Gamma function. Then the optimal number of bins \bar{m} can be derived through maximizing the above RLPP. For the observational light curve of Sgr A*, we find $m \sim 14$.

With the above binning, we can now construct χ^2 statistics for the CR distribution analysis:

$$\chi_{\text{CR}}^2 = (\mathbf{n}_{\text{obs}} - \mathbf{n}_{\text{sim}})^T \mathbf{C}^{-1} (\mathbf{n}_{\text{obs}} - \mathbf{n}_{\text{sim}}), \quad (5)$$

where the symbol T stands for the transpose of the matrix (vector), \mathbf{n}_{obs} and \mathbf{n}_{sim} are the vectors of the CR histogram values of the observed and simulated data, respectively. The covariance matrix \mathbf{C} is calculated according to N Monte Carlo realizations

$$C(i, j) = \frac{1}{N-1} \sum_{k=1}^N (n_i^k - \bar{n}_i)(n_j^k - \bar{n}_j), \quad (6)$$

where \bar{n}_i is the mean value of the i th bin of N realizations. The covariance matrix is involved here to account for the error correlations among different bins due to the correlated flare CRs (Brockwell & Davis 2010, and see discussions of the error estimation in Norberg et al. 2009). If there is no correlation between two histogram bins, $C(i, j) = \delta_{ij} \sigma_i^2$, Equation (5) is reduced to the standard definition of χ^2 . The exact value of N , as long as it is sufficiently large, has little effect on the calculation of the covariance matrix. In this work we adopt $N = 500$.

2.3.2. Structure Function

Following Emmanoulopoulos et al. (2010) we define the normalized SF as

$$V(\tau) = \frac{\langle [R(t + \tau) - R(t)]^2 \rangle}{S^2}, \quad (7)$$

where $R(t)$ is the CR as a function of time t , τ is the time lag, $\langle \rangle$ represents the average over the whole time range of the light curve, and S^2 is the variance of the CR

$$S^2 = \langle [R(t) - \overline{R(t)}]^2 \rangle. \quad (8)$$

This normalized SF is equivalent to the auto-correlation function as long as the time series is stationary, i.e., $\overline{R(t)} = \overline{R(t + \tau)} = \text{const.}$ (Emmanoulopoulos et al. 2010). The SF is especially suitable for the analysis of the data that are unequally sampled with large observational gaps, as is the case here.

Similar to the CR distribution, we build χ^2 statistics to compare the observed and simulated SFs quantitatively. Apart from the correlation among various SFs, which needs to be taken into account more seriously compared with the CR distribution, another issue for the standard definition of the χ^2 is that the random variable (the SF here) needs to be Gaussian. As shown in Emmanoulopoulos et al. (2010), the logarithm of the SF, instead of the SF itself, is approximately Gaussian.¹² The χ^2 statistic for the SF is thus defined as

$$\chi_{\text{SF}}^2 = (\log V_{\text{obs}} - \log V_{\text{sim}})^T C_{\text{SF}}^{-1} (\log V_{\text{obs}} - \log V_{\text{sim}}), \quad (9)$$

where the covariance matrix C_{SF} can be calculated the same way as Equation (6). The number of SF bins for the fitting procedure is chosen to be the same as that of the CR bins, i.e., $m = 14$. Note that the SF becomes a featureless plateau when the time lag is larger than the largest timescale of the flares. Correspondingly, the SF for the 14 bins are calculated between 300 s and 3×10^4 s.¹³ By minimizing $\chi^2 = \chi_{\text{CR}}^2 + \chi_{\text{SF}}^2$, we test our model and constrain the model parameters.

2.3.3. Model Fitting

We minimize $\chi^2 = \chi_{\text{CR}}^2 + \chi_{\text{SF}}^2$, using the MCMC method. It maps out the full posterior probability distributions and correlations of the model parameters. The MCMC code is adapted from the public CosmoMC code (Lewis & Bridle 2002). The Metropolis–Hastings algorithm (Metropolis et al. 1953; Hastings 1970), a propose-and-accept process in which the acceptance or rejection of a proposed point in the parameter space depends on the probability ratio between this point and the previous one, is adopted to generate the Markov chains.

¹² Although Emmanoulopoulos et al. (2010) show that the logarithm of the SF is only approximately Gaussian below a false break timescale related with its power spectrum, our Monte Carlo simulations suggest that $\log V(\tau)$ is indeed distributed roughly normally for the timescales considered here in spite of its ignorance of the location of the false break.

¹³ First, the SFs for the larger time delay τ will show remarkable fluctuations, and thus can be impossibly used for the fitting. second, we calculate the SFs with the observing gaps removed, which could introduce an artificial dip in the SFs when $\tau \gtrsim 8 \times 10^4$ s, corresponding to the typical timescale of the observing windows for the XVP data. However, the observing gaps show no significant effect on the SFs with $\tau \lesssim 3 \times 10^4$ s, the fitting range considered here.

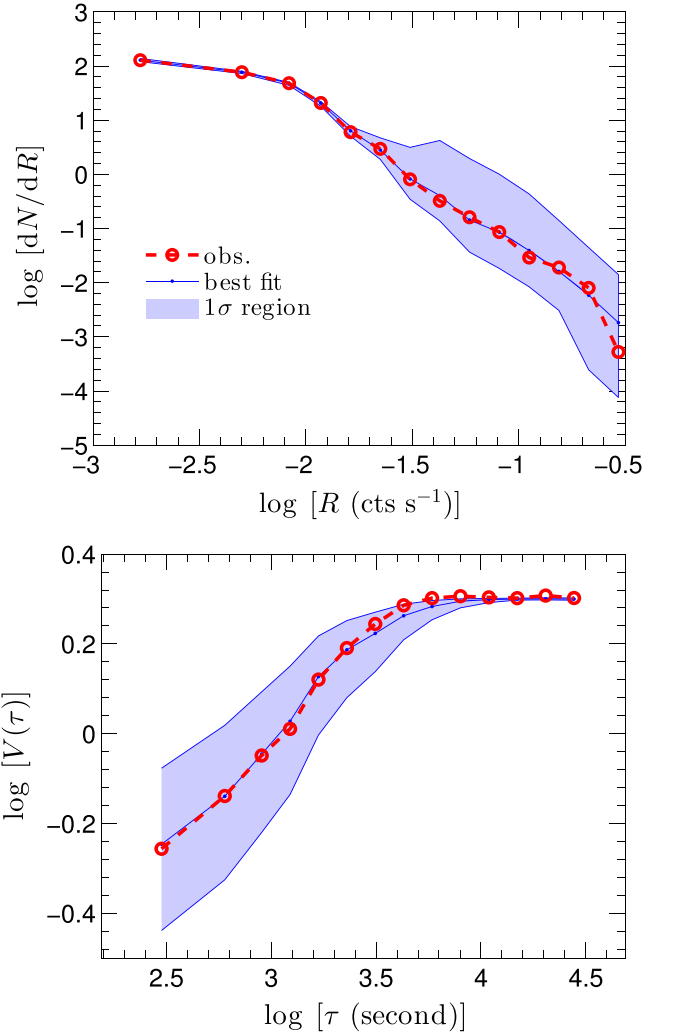


Figure 2. Upper panel: the CR distribution of the X-ray light curves of Sgr A*. The red circles are for the observed light curve, and blue dots are the best-fit model results. The bands show the fitting 1σ ranges of the CR distribution for the best-fit model according to the MCMC chains. Lower panel: the SF for the observed data and the simulations for the same parameter set.

3. RESULTS

3.1. Joint Fitting

The parameter σ_{ET} in the fittings is chosen to be 0.25, according to Q. Yuan et al. (2015, in preparation). Figure 2 shows the best-fit results and 1σ bands of the CR (upper panel) and the SF (lower panel), compared with the observations. The CR distribution exhibits an exponential distribution, which reflects the Poisson background, and a power-law tail, which represents the flares. The SF increases with τ and reaches a plateau of $\tau \sim 5 \times 10^3$ s, which corresponds to the largest duration of the flares. The profile with a rising trend clearly shows the timescale of the flares of the light curve. When the time lag τ is much longer than the largest timescale of the variabilities, the normalized SF asymptotically approaches 2, i.e., the plateau in Figure 2. It should be noted that the SF can be biased when applied to irregularly sampled light curves. In particular, the SF can show spurious breaks at $\Delta t \sim 10^{-1} \Delta T$, where ΔT is the total exposure time of the light curve (Emmanoulopoulos et al. 2010). However, the break seen here is at a much shorter timescale ($\sim 10^{-3} \Delta T$), and is consistent

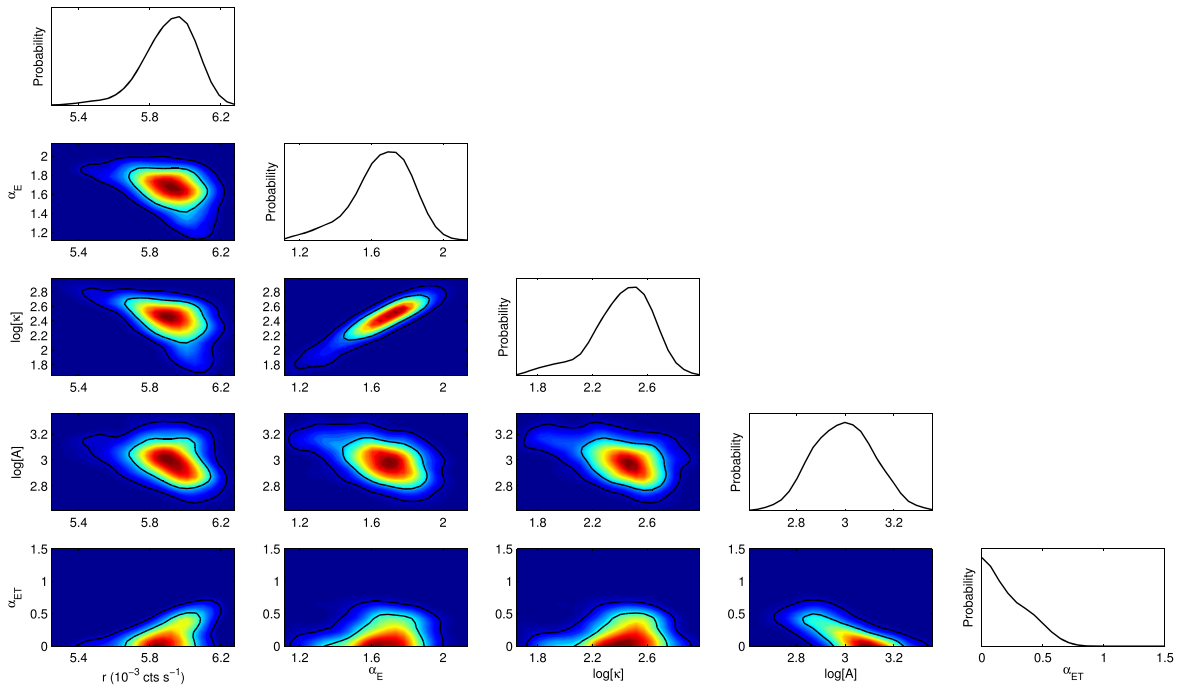


Figure 3. 1D and 2D probability distributions of the fitting parameters. The contours in the 2D plots are for confidence levels 68% and 95% from inside to outside, respectively.

with break timescales seen previously in both the NIR (Meyer et al. 2009; Witzel et al. 2012) and sub-millimeter (Dexter et al. 2014). Both of them suggest that the turnover time is likely an intrinsic characteristic timescale for the X-ray flares.

Figure 3 shows the one- and two-dimensional (1D and 2D) probability distributions of the parameters. The mean values and the 1σ uncertainties of the parameters are listed in Table 1. The fitting results suggest a fluence distribution power-law index $\alpha_E = 1.65 \pm 0.17$, and the less constrained fluence-duration correlation index $\alpha_{ET} < 0.55$ (95% confidence limit). The correlations between some of the parameters can be clearly seen in Figure 3. There is a strong correlation between the total number of flares κ and the fluence distribution index α_E . It is easy to understand that a harder fluence distribution will naturally correspond to a smaller number of flares in order not to over-produce the number of photons. Also the anti-correlation between α_E (or κ) and r is again due to the constraint of the total number of photon counts.

To judge the “goodness of fit” of the best-fit model, we use the bootstrapping method to estimate the confidence level. Based on the best-fit model parameter set as shown in Table 1, we generate 2000 realizations of the light curves and calculate the χ^2 values for each realization using the same method described in Section 2.3. The distribution of the χ^2 values is shown in Figure 4. The number fraction of realizations with χ^2 values smaller than that of the observational one, $\chi_{\text{obs}}^2 = 21$, is estimated to be 89.7%, indicating that the observed light curve is well characterized by the best-fit model.

Our preliminary re-analysis of the light curve indicates that the existing sample of flares may be biased against the detection of long duration ones. This bias can significantly affect the measurement of σ_{ET} and potentially other parameters as well. We have thus tested this latter sensitivity by fixing σ_{ET} to different values and found that the estimates of other parameters are not significantly altered (well within their

r (10^{-3} cts s^{-1})	α_E	$\log(\kappa)$	$\log(A)$	α_{ET}	χ^2_{ν}
5.90 ± 0.14	1.65	2.41	2.99 ± 0.12	< 0.55	0.9
	± 0.17	± 0.22			

Note. The errors are all 1σ (or 68%) confidence limit except for α_{ET} (for the one tail 95% confidence).

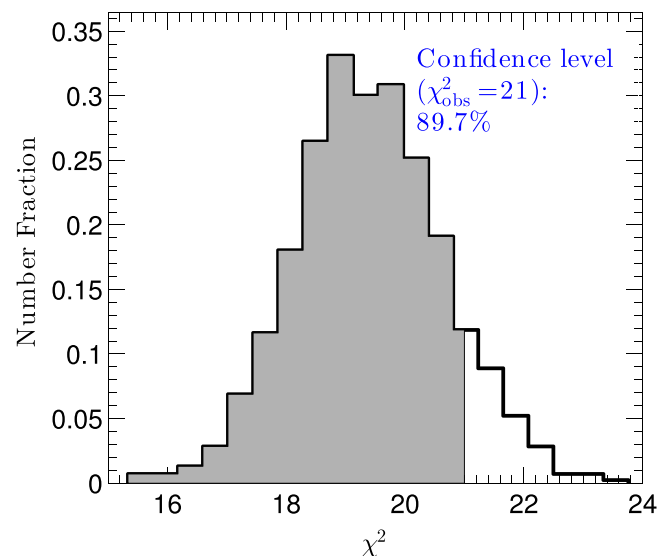


Figure 4. Distribution of χ^2 values of 2000 realizations of the light curves with the best-fit model parameters. The shaded region corresponds to a percentile of 89.7% for $\chi^2 < \chi_{\text{obs}}^2$.

uncertainties). The analysis, however, may be sensitive to the assumed specific shape of individual flares. We will address these potential higher-order complications in a follow-up paper.

3.2. Comparison with Previous Works

Neilsen et al. (2013) studied the statistical properties of the fluences, peak rates, durations, and luminosities of the 39 flares detected during the 2012 *Chandra* XVP. It was found that the distributions of the durations and luminosities can be well described by power-law functions, with indices $\alpha_T = 0.9 \pm 0.2$ and $\alpha_L = 1.9_{-0.3}^{+0.4}$, respectively. The power-law fittings to the fluence and peak rate distributions give $\alpha_E = 1.5 \pm 0.2$ and $\alpha_P = 1.9_{-0.4}^{+0.5}$. However, the fittings can be significantly improved by assuming cut-off power-law functions (Neilsen et al. 2013). Our result of α_E is consistent with that derived in Neilsen et al. (2013), even though only the detected sample was employed in the latter. Based on the Gaussian flare profile assumption, the slopes of the duration and peak rate distributions can be derived according to our fitting results,¹⁴ which are $\alpha_T \gtrsim 2.1$ and $1.7 \lesssim \alpha_P \lesssim 2.4$, respectively. The peak rate distribution is consistent with that of Neilsen et al. (2013), but the duration distribution is different. As mentioned above, the fluence–duration correlation derived in our work is also different from that of the detected sample. Possible reasons for these discrepancies include the incompleteness of the sample, and the profiles of the flares. Neilsen et al. (2015) showed that the flux distribution can be decomposed into two components, a steady Poisson background and a variable flare component. The X-ray flares excess follows a power-law process with $\alpha_F = 1.92_{-0.02}^{+0.03}$ and the Poisson background rate is $(5.24 \pm 0.08) \times 10^{-3}$ cts s⁻¹. The background rate derived here $(5.90 \pm 0.14) \times 10^{-3}$ cts s⁻¹ is slightly larger than that derived in Neilsen et al. (2015), possibly due to the different methods adopted. Although not shown explicitly, our result of Figure 2 gives roughly $\alpha_F \sim 2.2$, which is consistent with that of Neilsen et al. (2015). Wang et al. (2015) also analyzed the detected sample of Neilsen et al. (2013), with a different selection of the fitting data ranges, and found that $\alpha_E = 1.8 \pm 0.6$ and $\alpha_T = 1.9 \pm 0.5$.¹⁵ Within the large uncertainties, their results are consistent with what we obtain.

4. IMPLICATIONS ON THE NATURE OF THE FLARES

4.1. Confronting the Statistical Results with SOC Theory

We find that both the flare fluence distribution and the correlation between the duration and the fluence can be described by power laws, which is consistent with the prediction of the *fractal-diffusive SOC* theory (Aschwanden 2011, 2012, 2014). The SOC theory further predicts that the power-law indices will depend on the Euclidean space dimension S of the system to produce flares. The predicted power-law indices are $\alpha_E^{\text{th}} \approx 1.5$ and $\alpha_{\text{ET}}^{\text{th}} \approx 0.5$, respectively, for $S = 3$, the classical diffusion parameter $\beta = 1$, and the mean fractal dimension $D_S = (1 + S)/2$ (see the Appendix for more details). These values may vary in a range for different assumed values of β and D_S . For example, α_E can range from 1.4 to 1.7 for the fractal dimension $1 \leq D_{S=3} \leq 3$. Our results

¹⁴ For the duration distribution, since $T \propto E^{\alpha_{\text{ET}}}$, we have $\frac{dN}{dT} = \frac{dN}{dE} \cdot \frac{dE}{dT} \propto E^{-\alpha_E} \cdot E^{-\alpha_{\text{ET}}+1} \propto T^{-1-(\alpha_E-1)/\alpha_{\text{ET}}}$, and thus $\alpha_T = 1 + (\alpha_E - 1)/\alpha_{\text{ET}}$. For the peak CR distribution, $P \propto E/T \propto E/E^{\alpha_{\text{ET}}} = E^{1-\alpha_{\text{ET}}}$, then $\alpha_P = (\alpha_E - \alpha_{\text{ET}})/(1 - \alpha_{\text{ET}})$.

¹⁵ Concerning their analysis of Sgr A*, however, the flares sample is not corrected for the incompleteness, as well as the correlation of the uncertainties among different bins of the cumulative distributions are not properly addressed in the fittings.

of α_E and α_{ET} are actually in good agreement with the theoretical expectation with $S = 3$. The predicted indices of the duration and peak rate distributions are $\alpha_T^{\text{th}} \approx 2.0$ and $\alpha_P^{\text{th}} \approx 1.7$. As a comparison, our induced values are $\alpha_T \gtrsim 2.1$ and $1.7 \lesssim \alpha_P \lesssim 2.4$, respectively. There are potential discrepancies of these two distributions. Since the determination of the peak rate depends on the assumption of the flare profile, as well as the precise measurement of the flare duration, there should be relatively large uncertainty of the peak CR distribution. As shown in Nowak et al. (2012), the profile, at least for the bright ones, is indeed asymmetric rather than Gaussian. Therefore, the integral property (fluence) should be more reliably measured and more suitable to be used to compare with the theoretical model expectation.

4.2. Episodic Ejection of Plasma Blobs as Origin of Flares?

Two main conclusions can thus be obtained from the above analysis. First, the power-law distributions of the fluences, durations, and their correlation, suggest that the flares of Sgr A* can be explained in the *fractal-diffusive SOC* framework. Second, the inferred space dimension responsible for the flares is $S = 3$. Both results are similar to the solar flares, which thus implies that the X-ray flares of Sgr A* are likely driven by the similar physical mechanism as that of the solar flares. By analogy with the coronal mass ejections and their solar flares, Yuan et al. (2009) have proposed a magnetic reconnection model for the episodic ejections and the production of flares¹⁶ from the accretion flow of Sgr A*. In the following, we briefly review the key points of the model.

The structure of the accretion flow of Sgr A* is quite similar to the atmosphere of the Sun, i.e., a dense disk enveloped by a tenuous corona, as shown by the magneto-hydrodynamic simulations (e.g., Figure 4 in Yuan & Narayan 2014). The magnetic loops emerge into the disk corona due to the Parker instability. The configuration of the coronal magnetic field emerging from the accretion flow is controlled by the convective turbulence motion of the plasma in the disk. Since the foot points of the field lines are anchored in the accretion flow, which is turbulent and differentially rotating, a swamp of small-scale magnetic reconnection sets in, which redistributes the helicity and stores most of it in a flux rope. The turbulent processes in the accretion flow thus continuously build up magnetic stress and helicity. When a threshold is reached, e.g., when the current density inside the current sheet below the flux rope is strong enough, microscopic instabilities such as the two-streaming instability would be triggered, resulting in anomalous resistivity and fast magnetic reconnection inside the current sheet (Chen 2011). The equilibrium of the flux rope breaks down with accompanied dissipation of magnetic energy in a catastrophic manner, powering the observed flare. This is the so-called much-awaited SOC state which means that a small perturbation, owing to turbulence motion in accretion flow and subsequent magnetic reconnection, will trigger an avalanche-like chain reaction of any size in the system once the system self-organizes to a critical state.

5. CONCLUSIONS AND DISCUSSION

We present a statistical analysis to the *Chandra* 2–8 keV X-ray light curve of Sgr A* from the 3 Ms XVP campaign.

¹⁶ The flares and episodic ejections are physically associated with each other, both for the Sun and the black hole accretion flow.

A Monte Carlo simulation method is adopted to generate the model light curves, taking into account for the Poisson fluctuations of both the photon counts and the number of flares. We then fit the CR distribution and the SF of the light curves jointly to constrain the model parameters, via an MCMC method. We found that the X-ray emission of Sgr A* can be well modeled by two distinct components: a steady quiescent emission around the Bondi radius with a CR of $(5.90 \pm 0.14) \times 10^{-3}$ cts s^{-1} , and a flaring emission with a power-law fluence distribution $dN/dE \propto E^{-\alpha_E}$ with $\alpha_E = 1.65 \pm 0.17$. The duration-fluence correlation can also be modeled by a power-law form $T \propto E^{\alpha_{ET}}$ with $\alpha_{ET} < 0.55$.

These statistical properties are consistent with the theoretical predictions of the SOC system with the Euclid spatial dimension $S = 3$, same as that for solar flares (Aschwanden 2012, 2014). Our analysis, therefore, indicates that the X-ray flares of Sgr A* are possibly driven by the same physical mechanism as that of the solar flares, i.e., magnetic reconnection (Shibata & Magara 2011). This idea is further supported by the recent development of magneto-hydrodynamic simulations which lead to the consensus that the accretion flow in Sgr A* is enveloped by a tenuous corona above the dense disc (e.g., Yuan & Narayan 2014), similar to the atmosphere of the Sun. The three-dimensional geometry of the energy dissipation domain further suggests that the X-ray flaring of Sgr A* occurs in the surface of the accretion flow due to the less-ordered magnetic field structure embedded in it compared with that in the relativistic astrophysical jets (e.g., the GRBs; Wang & Dai 2013).

The flares of Sgr A* have also been detected in the NIR band (e.g., Genzel et al. 2003; Ghez et al. 2004). Dodds-Eden et al. (2011) and Witzel et al. (2012) analyzed the NIR flare data and found that the NIR flux distribution can also be described by a power-law form. However, the power-law indices obtained, which are -2.1 ± 0.6 (Dodds-Eden et al. 2011) and -4.2 ± 0.1 (Witzel et al. 2012), are different from each other. The cause for the discrepancy between these two results is unclear, and may be related to the subtractions of the stellar light. The former is roughly consistent with that of the X-ray flares (e.g., Neilsen et al. 2015, as well as our results in the context of the SOC framework with $S = 3$). If this is the case, then the NIR flares are expected to have the same physical origin as the X-ray flares, which is also supported by the results that NIR and X-ray flares occur simultaneously when there are coordinated observations at two wavebands (e.g., Dodds-Eden et al. 2009). Otherwise, it may suggest different radiation mechanisms between the NIR and X-ray flares which lead to the differences in the fractal dimension (Aschwanden 2011) or even different physical origins (Chan et al. 2015).

By analogy with solar flares, the multi-waveband flares of Sgr A* in X-ray, probably NIR, and less prominent sub-millimeter and radio, are likely associated with the ejection of plasmoids, both of which are the radiative manifestation of the common catastrophic phenomena (Yusef-Zadeh et al. 2006, 2008; Brinkerink et al. 2015). Such a result would be useful for understanding the origins of the flares and episodic jets in various black holes in general.

Mineshige et al. (1994b; see also Negoro et al. 1995; Takeuchi et al. 1995) studied the statistical properties of the X-ray fluctuations in Cygnus X-1, a black hole X-ray binary. They found that the X-ray fluctuations showed much steeper (or even exponential) distributions compared with those of

solar flares. They argued that the fluctuations should also follow an SOC process. A mass diffusion process was invoked in their works to explain the discrepancy of the distributions. But the X-ray fluctuations they discussed likely have a different physical origin compared with what we have discussed in the present paper. Thus the trigger mechanism of SOC is also different.

We thank all the members of the Sgr A* *Chandra* XVP collaboration (with PIs Fred Baganoff, Mike Nowak and Sera Markoff),¹⁷ and we are immensely grateful to *Chandra* Mission Planning for their support during our 2012 campaign. We thank F.Y. Wang, G. Witzel, S. Gillessen, D. Haggard, and S. Nayakshin for beneficial discussions. We would like to thank an anonymous referee for useful suggestions. Y.P.L. acknowledges the Graduate School of Xiamen University for the short term exchange program in University of Massachusetts Amherst. F.Y. was supported in part by the National Basic Research Program of China (973 Program, grant 2014CB845800), the Strategic Priority Research Program “The Emergence of Cosmological Structures” of CAS (grant XDB09000000), and NSF of China (grant 11133005). P.F.C. was supported in part by the National Basic Research Program of China (973 Program, grant 2011CB811402) and the NSF of China (grant 11025314).

APPENDIX SOC SYSTEM

The theoretical concept of SOC, proposed first by Katz (1986) and Bak et al. (1987) independently, describes a class of nonlinear dissipative dynamical systems that are slowly and continuously driven toward a critical value of an instability threshold, producing scale-free, fractal-diffusive, and intermittent avalanches (Charbonneau et al. 2001; Aschwanden 2011). The classical example of the SOC system is a sandpile (Bak et al. 1987). If one continuously drops the sand grains (driving force) to the same place, a conical sandpile will grow in a steady way until the surface shape reaches a critical slope, beyond which further addition of sand rapidly leads to catastrophic avalanches of the sandpile. The critical slope is primarily determined by the friction threshold between adjacent grains. Such a threshold is crucial since it allows the existence of multiple metastable states across the system. The continuous slow addition of sand will produce small or large avalanches with sizes independent of the input rate of sand. The critical behavior of the sandpile appears naturally as a consequence of the slow addition of sand without fine tuning of the addition rate. It is in this sense that the system is self-organized to criticality (Charbonneau et al. 2001; Aschwanden 2011). The continuous energy input (addition of sand) and nonlinear energy dissipation (avalanches due to the complicated interactions between the colliding sand grains) are two key points to determine whether a system is in an SOC state.

A universal property of the SOC system is that there is no preferred scale of the release of energy. The scale-free power-law distributions of various event parameters, which actually become the hallmarks of SOC systems, are expected. The ubiquitousness of power-law distributions in a wide range of physical systems, e.g., earthquakes, cloud formation, solar flares, and widely in astrophysics, suggests that SOC is a

¹⁷ <http://www.sgra-star.com/collaboration-members>

common law of nature. The SOC theory has been widely applied in geophysics (Turcotte 1999), solar physics (e.g., Charbonneau et al. 2001), and astrophysics (e.g., Mineshige et al. 1994a; Kawaguchi et al. 2000; Aschwanden 2011; Kunjaya et al. 2011).

The slope of the power-law form depends on how the subsystem self-organizes to the critical state. An analytic description was provided based on a *fractal-diffusive* avalanche model (Aschwanden 2012). The SOC state ensures that the entire system is close to the instability threshold, and the avalanches can develop in any direction once triggered. The propagation of the unstable nodes can thus be modeled with a random walk in an S -dimensional space (Aschwanden 2012). A statistical correlation between the spatial length scale L and time duration of the avalanche T for a diffusive random walk is predicted to be $L \propto T^{\beta/2}$, where β is a diffusion parameter ($\beta = 1$ corresponds to the classical diffusion). With the scale-free probability conjection $dN/dL \propto L^{-S}$, which means that the critical states are homogeneously distributed across the entire system, the occurrence frequency distributions of flare duration, flux, peak flux, and total energy can be obtained in the *fractal-diffusive* avalanche model (Aschwanden 2012). The indices of the total energy (fluence) α_E^{th} , duration α_T^{th} , peak luminosity (or peak CR in this work) α_P^{th} , and flux (or CR) α_F^{th} distributions are derived as (Aschwanden 2012, 2014)

$$\alpha_E^{\text{th}} = 1 + \frac{S-1}{D_S + 2/\beta}, \quad (10)$$

$$\alpha_T^{\text{th}} = 1 + \frac{(S-1)\beta}{2}, \quad (11)$$

$$\alpha_P^{\text{th}} = 1 + \frac{S-1}{S}, \quad (12)$$

$$\alpha_F^{\text{th}} = 1 + \frac{S-1}{D_S}, \quad (13)$$

where S is the Euclidean space dimension, D_S is the fractal Hausdorff dimension, which lies between 1 and S . The *fractal-diffusive* SOC theory also predicts the scaling relations between various flare parameters. The correlation slope between the total energy E and duration T is (Aschwanden 2012, 2014)

$$\alpha_{ET}^{\text{th}} = \frac{2}{D_S\beta + 2}. \quad (14)$$

For the classical diffusion ($\beta = 1$) and an estimated mean fractal dimension of $D_S \approx (S+1)/2$, we have $\alpha_E^{\text{th}} = 1.5$, $\alpha_T^{\text{th}} = 2.0$, $\alpha_P^{\text{th}} = 1.7$, $\alpha_F^{\text{th}} = 2.0$, and $\alpha_{ET}^{\text{th}} = 0.5$ for $S = 3$.

REFERENCES

- Aharonian, F., Akhperjanian, A. G., Barres de Almeida, U., et al. 2008, *A&A*, **492**, L25
- Aschwanden, M. J. 2011, *Self-Organized Criticality in Astrophysics*, ed. M. J. Aschwanden (Berlin: Springer)
- Aschwanden, M. J. 2012, *A&A*, **539**, A2
- Aschwanden, M. J. 2014, *ApJ*, **782**, 54
- Aschwanden, M. J., & McTiernan, J. M. 2010, *ApJ*, **717**, 683
- Baganoff, F. K., Bautz, M. W., Brandt, W. N., et al. 2001, *Natur*, **413**, 45
- Baganoff, F. K., Maeda, Y., Morris, M., et al. 2003, *ApJ*, **591**, 891
- Bak, P., Tang, C., & Wiesenfeld, K. 1987, *PhRvL*, **59**, 381
- Barrière, N. M., Tomsick, J. A., Baganoff, F. K., et al. 2014, *ApJ*, **786**, 46
- Béanger, G., Goldwurm, A., Melia, F., et al. 2005, *ApJ*, **635**, 1095
- Brinkerink, C. D., Falcke, H., Law, C. J., et al. 2015, *A&A*, **576**, A41
- Brockwell, P. J., & Davis, R. A. 2010, in *Introduction to Time Series and Forecasting*, ed. P. J. Peter & R. A. Davis (2nd ed.; New York: Springer), 2002
- Broderick, A. E., & Loeb, A. 2005, *MNRAS*, **363**, 353
- Chan, C.-K., Psaltis, D., Ozel, F., et al. 2015, *ApJ*, submitted (arXiv:1505.01500)
- Charbonneau, P., McIntosh, S. W., Liu, H.-L., & Bogdan, T. J. 2001, *SoPh*, **203**, 321
- Chen, P. F. 2011, *LRSF*, **8**, 1
- Degenaar, N., Miller, J. M., Kennea, J., et al. 2013, *ApJ*, **769**, 155
- Dexter, J., Kelly, B., Bower, G. C., et al. 2014, *MNRAS*, **442**, 2797
- Dodds-Eden, K., Gillessen, S., Fritz, T. K., et al. 2011, *ApJ*, **728**, 37
- Dodds-Eden, K., Porquet, D., Trap, G., et al. 2009, *ApJ*, **698**, 676
- Dodds-Eden, K., Sharma, P., Quataert, E., et al. 2010, *ApJ*, **725**, 450
- Eckart, A., Baganoff, F. K., Schödel, R., et al. 2006, *A&A*, **450**, 535
- Emmanoulopoulos, D., McHardy, I. M., & Uttley, P. 2010, *MNRAS*, **404**, 931
- Genzel, R., Eisenhauer, F., & Gillessen, S. 2010, *RvMP*, **82**, 3121
- Genzel, R., Schödel, R., Ott, T., et al. 2003, *Natur*, **425**, 934
- Ghez, A. M., Wright, S. A., Matthews, K., et al. 2004, *ApJL*, **601**, L159
- Hastings, W. K. 1970, *Biometrika*, **57**, 97
- Katz, J. I. 1986, *JGR*, **91**, 10412
- Kawaguchi, T., Mineshige, S., Machida, M., Matsumoto, R., & Shibata, K. 2000, *PASJ*, **52**, L1
- Knuth, K. H. 2006, arXiv:physics/0605197
- Kunjaya, C., Mahasena, P., Vierdayanti, K., & Herlie, S. 2011, *Ap&SS*, **336**, 455
- Lewis, A., & Bridle, S. 2002, *PhRvD*, **66**, 103511
- Li, J., Ostriker, J. P., & Sunyaev, R. 2013, *ApJ*, **767**, 105
- Lin, J., & Forbes, T. G. 2000, *JGR*, **105**, 2375
- Lu, E. T., & Hamilton, R. J. 1991, *ApJL*, **380**, L89
- Markoff, S., Falcke, H., Yuan, F., & Biermann, P. L. 2001, *A&A*, **379**, L13
- Marrone, D. P., Baganoff, F. K., Morris, M. R., et al. 2008, *ApJ*, **682**, 373
- Metropolis, N., Rosenbluth, A. W., Rosenbluth, M. N., Teller, A. H., & Teller, E. 1953, *JChPh*, **21**, 1087M
- Meyer, L., Do, T., Ghez, A., et al. 2009, *ApJL*, **694**, L87
- Mineshige, S., Ouchi, N. B., & Nishimori, H. 1994a, *PASJ*, **46**, 97
- Mineshige, S., Takeuchi, M., & Nishimori, H. 1994b, *ApJL*, **435**, L125
- Narayan, R., Sądowski, A., Penna, R. F., & Kulkarni, A. K. 2012, *MNRAS*, **426**, 3241
- Negoro, H., Kitamoto, S., Takeuchi, M., & Mineshige, S. 1995, *ApJL*, **452**, L49
- Neilsen, J., Markoff, S., Nowak, M. A., et al. 2015, *ApJ*, **799**, 199
- Neilsen, J., Nowak, M. A., Gammie, C., et al. 2013, *ApJ*, **774**, 42
- Norberg, P., Baugh, C. M., Gaztañaga, E., & Croton, D. J. 2009, *MNRAS*, **396**, 19
- Nowak, M. A., Neilsen, J., Markoff, S. B., et al. 2012, *ApJ*, **759**, 95
- Porquet, D., Grosso, N., Predehl, P., et al. 2008, *A&A*, **488**, 549
- Porquet, D., Predehl, P., Aschenbach, B., et al. 2003, *A&A*, **407**, L17
- Priest, E., & Forbes, T. 2000, *Magnetic Reconnection: MHD Theory and Applications* (New York: Cambridge Univ. Press)
- Shibata, K., & Magara, T. 2011, *LRSF*, **8**, 6
- Simonetti, J. H., Cordes, J. M., & Heeschen, D. S. 1985, *ApJ*, **296**, 46
- Tagger, M., & Melia, F. 2006, *ApJL*, **636**, L33
- Takeuchi, M., Mineshige, S., & Negoro, H. 1995, *PASJ*, **47**, 617
- Trap, G., Goldwurm, A., Dodds-Eden, K., et al. 2011, *A&A*, **528**, A140
- Turcotte, D. L. 1999, *RPPH*, **62**, 1377
- Wang, F. Y., & Dai, Z. G. 2013, *NatPh*, **9**, 465
- Wang, F. Y., Dai, Z. G., Yi, S. X., & Xi, S. Q. 2015, *ApJS*, **216**, 8
- Wang, Q. D. 2004, *ApJ*, **612**, 159
- Wang, Q. D., Nowak, M. A., Markoff, S. B., et al. 2013, *Sci*, **341**, 981
- Witzel, G., Eckart, A., Bremer, M., et al. 2012, *ApJS*, **203**, 18
- Yuan, F., Bu, D., & Wu, M. 2012, *ApJ*, **761**, 130
- Yuan, F., Lin, J., Wu, K., & Ho, L. C. 2009, *MNRAS*, **395**, 2183
- Yuan, F., & Narayan, R. 2014, *ARA&A*, **52**, 529
- Yuan, F., Quataert, E., & Narayan, R. 2003, *ApJ*, **598**, 301
- Yuan, F., Quataert, E., & Narayan, R. 2004, *ApJ*, **606**, 894
- Yusef-Zadeh, F., Bushouse, H., Wardle, M., et al. 2009, *ApJ*, **706**, 348
- Yusef-Zadeh, F., Roberts, D., Wardle, M., Heinke, C. O., & Bower, G. C. 2006, *ApJ*, **650**, 189
- Yusef-Zadeh, F., Wardle, M., Heinke, C., et al. 2008, *ApJ*, **682**, 361
- Zubovas, K., Nayakshin, S., & Markoff, S. 2012, *MNRAS*, **421**, 1315